Mon. Not. R. Astron. Soc. **349,** 1052–1058 (2004) doi:10.1111/j.1365-2966.2004.07583.x

Merging of low-mass systems and the origin of the Fundamental Plane

E. A. Evstigneeva,[1⋆†] R. R. de Carvalho,[2] A. L. Ribeiro[3] and H. V. Capelato[4]

[1]*Astronomical Institute of St Petersburg State University, 198504 St Petersburg, Russia*
[2]*Observatório Nacional, 20921-400 Rio de Janeiro, Brazil*
[3]*Universidade Estadual de Santa Cruz, 45650-000 Ilheus-BA, Brazil*
[4]*Divisão de Astrofísica - INPE/MCT CP 515, 12201-970 SP, Brazil*

Accepted 2003 December 30. Received 2003 December 22; in original form 2003 October 14

ABSTRACT

We present a new set of dissipationless *N*-body simulations to examine the feasibility of creating bright ellipticals (following the Kormendy relation, hereafter KR) by hierarchically merging present-day early-type dwarf galaxies, and to study how the encounter parameters affect the location of the end product in the $\langle\mu_e\rangle$–R_e plane. We investigate the merging of one-component galaxies of both equal and different masses, the merging of two-component galaxy models to explore the effect of dark haloes on the final galaxy characteristics, and the merging of ultracompact dwarf galaxies. We find that the increase of $\langle\mu_e\rangle$ with R_e is attributable to an increase in the initial orbital energy. The merger remnants shift down in the $\langle\mu_e\rangle$–R_e plane and fail to reach the KR. Thus, the KR is not reproducible by mergers of dwarf early-type systems, rendering untenable the theory that present-day dwarfs are responsible for even a small fraction of the present-day ellipticals, unless a considerable amount of dissipation is invoked. However, we do find that present-day dwarfs can be formed by the merger of ultracompact dwarfs.

Key words: methods: numerical – galaxies: dwarf – galaxies: elliptical and lenticular, cD – galaxies: formation – galaxies: fundamental parameters.

1 INTRODUCTION

Despite the progress made in understanding the physics of early-type galaxies, a single widely accepted formation model, capable of explaining all their observed properties, does not yet exist. There is a variety of scenarios describing how these objects were formed, ranging from the collapse of clumpy protogalaxies (Eggen, Lynden-Bell & Sandage 1962; Larson 1975) to the merging of smaller galaxies (White & Rees 1978; Kauffmann 1996; Cole et al. 2000). Nevertheless, the remarkable fact is that early-type galaxies demonstrate a very tight kinematic-structural relationship, usually referred to as the Fundamental Plane (Djorgovski & Davis 1987; Dressler et al. 1987), and any theory of galaxy formation and evolution must be able to account for its tightness and environmental independence (de la Rosa, de Carvalho & Zepf 2001).

The Fundamental Plane (FP) combines photometric parameters (R_e, the effective radius, along with $\langle\mu_e\rangle$, the mean surface brightness within R_e) with a spectroscopic observable (the line-of-sight central velocity dispersion σ_0). The measured values of R_e, μ_e and σ_0 for a sample of E and S0 galaxies fill a thin plane (with scatter of ∼0.1 dex) within this three-parameter space instead of spreading out over the whole space. The FP can be projected on to any pair of axes from the three variables. Examples of these projections are the Kormendy relation, $\mu_e - \log R_e$ (Kormendy 1977), and the Faber–Jackson relation between luminosity and central velocity dispersion (Faber & Jackson 1976).

The distribution of elliptical galaxies in the $\langle\mu_e\rangle$–R_e plane, shown in Fig. 1, reveals the existence of two distinct families: the 'ordinary' family, composed of early-type dwarfs, lying in the region defined by $22 \leqslant \langle\mu_e(B)\rangle \leqslant 27$ and $R_e \leqslant 3$ kpc and which are always fainter than $M(B) = -19.3$, and the 'bright' family, containing the most luminous elliptical galaxies (the brightest cluster galaxies – BCGs, which host QSOs and Seyfert nuclei), populating a relatively narrow strip in the $\langle\mu_e\rangle$–R_e plane, with $M(B) < -19.3$ and extending over 2 dex in R_e. The presence of boxy isophotes in these luminous galaxies and the high frequency of multiple nuclei among BCGs lends support to the merging scenario for the 'bright' family. The low-luminosity discy ellipticals occupy the region between dwarfs and bright elliticals in the $\langle\mu_e\rangle$–R_e plane [$-0.5 \lesssim \log R_e \lesssim 0.7$, $18 \lesssim \langle\mu_e(B)\rangle \lesssim 23$]. We did not show them in the figure to avoid confusion. Capaccioli, Caon & D'Onofrio (1992) interpreted the $\langle\mu_e\rangle$–R_e plane for ellipticals as a logical equivalent to the HR diagram for stars, and that galaxies might reach the 'bright' end of this diagram through successive mergers of low-mass systems.

The segregation of galaxies in the $\langle\mu_e\rangle$–R_e plane, together with the different behaviour of dEs and luminous elliptical galaxies (Es) in the $M(B)$–$\langle\mu_e\rangle$ diagram, where $M(B)$ is the absolute magnitude

⋆E-mail: katya@physics.uq.edu.au
†Present address: Department of Physics, University of Queensland, QLD 4072, Australia.

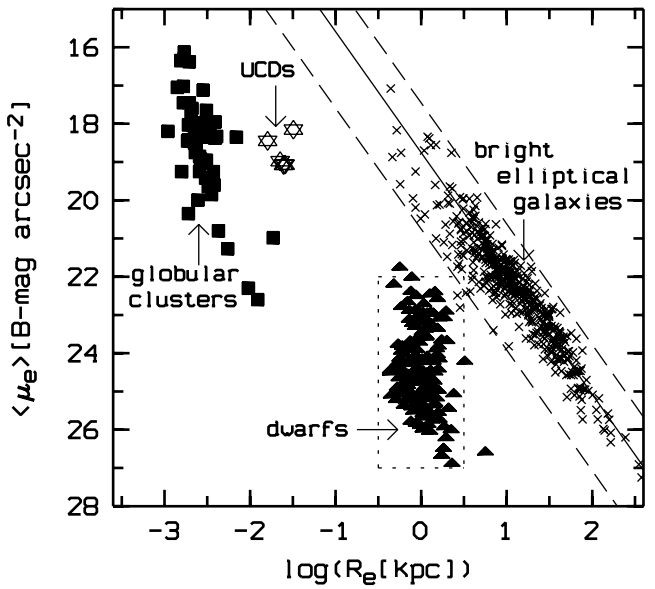

Figure 1. The $\langle\mu_e\rangle$–R_e plane for different types of objects. Filled triangles and crosses are data from Capaccioli et al. (1992). Filled squares are globular clusters from Burstein et al. (1997). Starred symbols are ultracompact dwarf galaxies from Drinkwater et al. (2003). The solid line represents the Kormendy relation. Both dashed lines represent the locii of families exhibited in this diagram. They schematically represent their overall extension.

(see Graham & Guzman 2003), was generally interpreted as evidence for distinct formation and/or evolutionary processes for the two families of objects. However, there is evidence for a continuity, rather than dichotomy, between Es and dEs. According to Graham & Guzman (2003), dE galaxies form a continuous sequence with the brighter E galaxies, such that μ_0 (the central surface brightness) brightens linearly with $M(B)$ until core formation causes the most luminous E galaxies ($M(B) \leqslant -20.5$) to deviate from this relation. The different behaviour of dE and E galaxies in the $M(B)$–$\langle\mu_e\rangle$ [or $M(B)$–μ_e] diagram and the $\langle\mu_e\rangle$–R_e plane,is unrelated to core formation, and is expected from the continuous and linear relation between $M(B)$ and μ_0, and $M(B)$ and log(n) (the Sersic index).

In hierarchical galaxy formation scenarios (as in the CDM model), small galaxies (or dark matter haloes) are the building blocks of more massive galaxies, and should have been more numerous in the early Universe. Thus, the present-day dwarfs can be seen as survivors of an initially much richer population. However, we observe many fewer dwarfs today than the predicted number of surviving dark matter haloes (Klypin et al. 1999; Moore et al. 1999). There also appear to be inconsistencies in the time-scales necessary to construct large galaxies (Prantzos & Silk 1998), and differences in the stellar populations of large and small galaxies (Tolstoy et al. 2003). These problems point to a need to better understand the physics of dwarf galaxies.

In the present paper, we concentrate on a single aspect of the complex properties of this family of galaxies, the dwarf ellipticals found in the lower left corner of Fig. 1 ($\langle\mu_e(B)\rangle \geqslant 22$ and $R_e \leqslant$ 3 kpc). Dwarf ellipticals (dEs) are spherical or elliptical in appearance, compact, with high central stellar densities. They are fainter than $M(B) = -18$ and have low masses ($M_{tot} \leqslant 10^9$ M$_\odot$). They are found preferentially in the vicinity of massive galaxies, usually have little or no detectable gas, and are often not rotationally supported. When gas is detected, it exhibits an asymmetric distribution, is less extended than the underlying stellar component, and seems to be kinematically distinct (see Grebel 2001, and references therein). dEs sometimes show pronounced nuclei, with the fraction of nucleated dEs increasing with luminosity. The surface density profiles of dEs are best described by Sersic's generalization of de Vaucouleurs $R^{1/4}$ law and exponential profiles (see Grebel 2001, and references therein). The origin of these early-type dwarfs is still unknown. Three general classes of models have been suggested (Grebel, Gallagher & Harbeck 2003): tidal interactions that transform field disc galaxies into spheroidal systems; processes associated with the birth of small systems (in the CDM model); and fragments torn from collisions between larger galaxies. However, each of these models encounter certain difficulties in reproducing the observed properties of dEs.

The effects of dissipationless merging on the FP have been explored in Capelato, de Carvalho & Carlberg (1995), Dantas et al. (2003) and Nipoti, Londrillo & Ciotti (2003), among others. In these contributions, the progenitors lay on the FP, and the edge-on projection of the FP was found to be reproduced by dissipationless merging. In contrast to these works, our initial models are low-mass early-type galaxies which lie neither on the FP nor along the Kormendy Relation (KR). We consider the merging of one-component galaxies of both equal and different masses, as well as the merging of two-component galaxy models, to explore the effects of dark haloes on the final galaxy characteristics. We also examine mergers of ultracompact dwarf galaxies (UCDs), as these constitute a recently discovered class of very compact objects (Drinkwater et al. 2000; Bekki et al. 2001), populating the FP in a previously empty region between the most luminous globular clusters and nucleated dwarf galaxies.

To form a complete picture and compare our results with those obtained by other authors, we run a series of simulations where the progenitor models lie on the KR. We also merge objects that lie above the KR in the $\langle\mu_e\rangle$–R_e plane. These objects are not found in the nearby Universe, but may have existed at earlier epochs, and are probable progenitors for present-day ellipticals.

2 NUMERICAL METHOD AND INPUT

2.1 The numerical code

Our computations utilize an N-body code with a hierarchical tree algorithm and multipole expansion to compute the forces, as proposed by Barnes & Hut (1986). The force computation includes the quadrupole correction terms, following Dubinski (1988).

The set of input parameters (ϵ, the potential softening length; N, the number of particles; Δt, the integration time-step) used in the various simulations are listed in Table 1. Also given in this table are the upper limits of the relative variation of the total energy, E, and the relative variation of the total angular momentum, J, for simulations using each set of parameters. The tolerance parameter was the same for all simulations, $\theta = 0.8$. As discussed in Dantas et al. (2002), the choice of the softening parameter ϵ is a compromise between spatial resolution and the collisionless condition of the system on evolutionary time-scales. It thus depends on the particle number N, and on the specific density distribution profile (see also e.g. Merritt 1996).

2.2 Galaxy models

We measure mass and length in units of 10^8 M$_\odot$ and 1 kpc, respectively. These values, together with the gravitational constant

Table 1. The initial simulation parameters and the relative variations of the total energy and the total angular momentum.

	ϵ	Δt	N	M	$\Delta E/E$ per cent	$\Delta J/J$ per cent
Low-mass systems:						
One-component equal mass merging	$\epsilon_{1,2} = 0.07$	0.025	$N_{1,2} = 90\,000$	$M_{1,2} = 9$	0.4	2.8
One-component different mass merging	$\epsilon_1 = 0.09$ $\epsilon_2 = 0.13$	0.1	$N_1 = 90\,000$ $N_2 = 30\,000$	$M_1 = 9$ $M_2 = 3$	0.7	2.3
UCDs	$\epsilon_{1,2} = 0.002$	0.001	$N_{1,2} = 30\,000$	$M_{1,2} = 0.6$	5.0	2.0
Two-component equal mass merging	$\epsilon_s = 0.15$ $\epsilon_h = 0.40$	0.15	$N_s = 20\,000$ $N_h = 60\,000$	$M_s = 9$ $M_h = 27$	2.5	1.5
Merging of ellipticals lying on the KR	$\epsilon_{1,2} = 0.07$	0.005	$N_{1,2} = 90\,000$	$M_{1,2} = 2\,229$	3.0	1.8
Merging of objects lying above the KR	$\epsilon_{1,2} = 0.07$	0.001	$N_{1,2} = 180\,000$	$M_{1,2} = 35\,218$	1.3	4.0

$G = 1$, fix our time and velocity units as 47.2 Myr and 20.7 km s^{-1}, respectively.

The initial models for merging of low-mass galaxies were chosen from the region in Fig. 1 occupied by ordinary ellipticals and early-type dwarfs (the 'ordinary' group). Both one- and two-component models were constructed as described below.

The initial one-component galaxies were modelled using the potential-density pair for spherical galaxies given in Hernquist (1990):

$$\Phi(r) = -\frac{GM}{r+a}, \tag{1}$$

$$\rho(r) = \frac{M}{2\pi a^3}\frac{a^4}{r(r+a)^3}, \tag{2}$$

where M is the galaxy mass and a is the scalelength.

In the case of two-component models (the luminous galaxy and its dark matter halo), the halo density profile was represented as a truncated isothermal sphere (Hernquist 1993):

$$\rho(r) = \frac{M_h}{2\pi^{3/2}}\frac{\alpha}{r_c}\frac{\exp\left(-r^2/{r_c}^2\right)}{r^2+\gamma^2}. \tag{3}$$

Here M_h is the halo mass, γ is the core radius and r_c is the cut-off radius. The normalization constant α is defined by

$$\alpha = (1 - \sqrt{\pi}q\exp(q^2)[1 - erf(q)])^{-1}, \tag{4}$$

where $q = \gamma/r_c$. The cumulative mass profile, $M_h(r)$, and potential, $\Phi(r)$, corresponding to $\rho(r)$ are

$$M_h(r) = \frac{2M_h\alpha}{\sqrt{\pi}}\int_0^{r/r_c}\frac{x^2\exp(-x^2)}{x^2+q^2}\mathrm{d}x, \tag{5}$$

$$\Phi_h(r) = -\frac{GM_h(r)}{r} + \frac{GM_h(r)\alpha}{\sqrt{\pi}r_c}Ei[-(r/r_c)^2 - q^2], \tag{6}$$

where $Ei(z)$ is an exponential integral.

We constructed single-component models representing early-type dwarfs galaxies with total masses of $M_{dw_1} = 9$ and $M_{dw_2} = 3$, both having the same scalelength $a = 1$ ($R_e \approx 1.8\,a$).

The two-component model for early-type dwarfs consists of a luminous component identical to that for the one-component dw_1 model described above, with the dark matter halo more massive ($M_h/M_s = 3$) and less concentrated ($\gamma/a = 3$) than the stellar component. The dark component parameters for these models are $M_h = 27$, $\gamma = 3$ and $r_c = 12$. Given the lack of observational data on dark matter in dwarf galaxies, these models are consistent with current ideas on the structure of these objects.

The effective radii of UCDs range from 0.015 kpc ($\log R_e = -1.82$) to 0.03 kpc ($\log R_e = -1.52$) and their mean surface brightness within R_e ranges from 18 to 19. The UCD radial profiles are well described by de Vaucouleurs profiles (Drinkwater et al. 2003). For the initial UCD models, we used a Hernquist sphere with $M_{ucd} = 0.6$ and $a_{ucd} = 0.014$.

Finally, for the progenitor models lying on and above the KR, we constructed models with $M_{KR} = 2229$, and $M_{AKR} = 35218$, respectively, with both models having $a = 1$.

2.3 Initial conditions

The encounter of two non-rotating spherical galaxies may be characterized by the dimensionless energy and angular momentum:

$$\hat{E} = \frac{E_{orb}}{\frac{1}{2}\mu\overline{\langle v^2\rangle}}, \tag{7}$$

$$\hat{L} = \frac{L_{orb}}{\mu\overline{r_h}\overline{\langle v^2\rangle}^{\frac{1}{2}}}, \tag{8}$$

where $\overline{\langle v^2\rangle} = \sqrt{\langle v_1^2\rangle\langle v_2^2\rangle}$, $r_h = \sqrt{r_{h1}r_{h2}}$. Here $\langle v^2\rangle$ is the internal mean-square velocity, r_h is the half-mass radius of a galaxy (Binney & Tremaine 1987). The indices denote each of the initial galaxies and μ is the reduced mass of the system.

The time required for two galaxies to merge is a function of the initial position of the binary orbit in the $(\hat{E}, \hat{L})$ plane defined by equations (7) and (8) (Binney & Tremaine 1987). We considered only those pairs of $(\hat{E}, \hat{L})$ which correspond to rapid mergers (less than a Hubble time).

To determine the orbital elements of the encounter completely, we must define a third parameter:

$$A = \frac{2GM}{\overline{r_h}\overline{\langle v^2\rangle}}, \tag{9}$$

which depends only on the dynamical structure of the initial galaxies. The initial separations and velocities for the encounters are selected from a grid of $\hat{E}$, $\hat{L}$, A values. The initial separation of the models was taken at the apocenter position for bound orbits and $\sim 4r_h$ for unbound ones.

We follow the dynamical evolution of each merger until the resulting system is virialized, which typically occurs on a time-scale shorter than $20T_{cr}$ after the first encounter between two galaxies, where T_{cr} is the crossing time of the final object

Table 2. Merging of one-component equal mass models.

Run	$\hat{E}$	$\hat{L}$	$T_{\rm per}$	$20T_{\rm cr}$	$T_{\rm end}$	log $R_{\rm e}$ (kpc)	$\langle\mu_{\rm e}\rangle$
Progenitor (dw_1)						0.19 ± 0.00	25.00 ± 0.01
E01	-3	0	4.2	144	275	0.43 ± 0.02	25.48 ± 0.11
E02	-7	0	4.3	100	100	0.34 ± 0.02	25.00 ± 0.10
E03	-5	0	5.3	119	121	0.38 ± 0.02	25.23 ± 0.12
E04	-3	1	24.3	140	150	0.43 ± 0.02	25.50 ± 0.11
E05	-5	1	11.3	117	120	0.38 ± 0.03	25.21 ± 0.13
E06	-7	1	6.8	102	120	0.34 ± 0.02	25.02 ± 0.10
E07	-3	2	24.3	140	150	0.43 ± 0.02	25.46 ± 0.11
E08	-5	2	11.6	91	150	0.38 ± 0.02	25.20 ± 0.10
E09	-7	2	6.8	102	175	0.34 ± 0.02	25.00 ± 0.10
E10	-1	3	126.3	174	200	0.47 ± 0.02	25.70 ± 0.12
E11	0	1	2.6	166	170	0.49 ± 0.03	25.87 ± 0.15
E12	0.5	1	2.5	178	182	0.49 ± 0.03	25.87 ± 0.15
E13	1	1	2.5	191	200	0.50 ± 0.03	25.95 ± 0.14
$E01_2$	-3	0	5.8	193	234	0.62 ± 0.03	26.76 ± 0.16
$E02_2$	-7	0	4.2	82	150	0.47 ± 0.05	24.93 ± 0.24
$E05_2$	-5	1	11.6	109	150	0.54 ± 0.04	25.27 ± 0.20
$E06_2$	-7	1	7.0	83	125	0.46 ± 0.04	24.87 ± 0.18
$E08_2$	-5	2	11.6	96	231	0.55 ± 0.04	25.33 ± 0.20
$E09_2$	-7	2	7.0	83	150	0.47 ± 0.04	24.90 ± 0.19
$E01_3$	-3	0	8.9	416	546	0.83 ± 0.03	26.19 ± 0.17
$E02_3$	-7	0	4.2	85	150	0.59 ± 0.05	24.78 ± 0.26
$E05_3$	-5	1	11.6	84	200	0.71 ± 0.04	25.37 ± 0.22
$E06_3$	-7	1	7.0	134	359	0.58 ± 0.05	24.71 ± 0.24
$E09_3$	-7	2	7.0	87	300	0.59 ± 0.06	24.75 ± 0.27

Table 3. Merging of one-component different mass progenitors.

Run	$\hat{E}$	$\hat{L}$	$T_{\rm per}$	$20T_{\rm cr}$	$T_{\rm end}$	log $R_{\rm e}$ (kpc)	$\langle\mu_{\rm e}\rangle$
Progenitor1 (dw_1)						0.19 ± 0.00	25.00 ± 0.01
Progenitor2 (dw_2)						0.18 ± 0.00	26.16 ± 0.01
D01	-3	1	35.0	110	164	0.36 ± 0.02	25.60 ± 0.10
D02	-5	1	16.3	99	152	0.34 ± 0.02	25.46 ± 0.09
D03	-7	1	9.9	91	137	0.30 ± 0.01	25.28 ± 0.07
D04	-3	2	35.0	110	164	0.36 ± 0.02	25.58 ± 0.10
D05	-5	2	16.3	100	152	0.33 ± 0.02	25.44 ± 0.09
D06	-7	2	9.8	92	140	0.30 ± 0.02	25.28 ± 0.08

Table 4. Merging of ultracompact dwarf galaxies.

Run	$\hat{E}$	$\hat{L}$	$T_{\rm per}$	$20T_{\rm cr}$	$T_{\rm end}$	log $R_{\rm e}$ (kpc)	$\langle\mu_{\rm e}\rangle$
Progenitor (ucd)						-1.65 ± 0.00	18.75 ± 0.01
F01	-1	1	0.84	0.96	2.0	-1.32 ± 0.03	19.69 ± 0.13
$F01_2$	-1	1	1.80	1.80	4.0	-1.03 ± 0.04	20.44 ± 0.21
$F01_3$	-1	1	3.22	3.55	7.3	-0.74 ± 0.05	21.14 ± 0.23
$F01_4$	-1	1	5.78	6.82	18.5	-0.47 ± 0.04	21.80 ± 0.22

Table 5. Merging of two equal-mass progenitors with dark halo.

Run	$\hat{E}$	$\hat{L}$	$T_{\rm per}$	$20T_{\rm cr}$	$T_{\rm end}$	log $R_{\rm e}$ (kpc)	$\langle\mu_{\rm e}\rangle$
Progenitor						0.19 ± 0.00	25.01 ± 0.01
H01	-3	1	55.8	245	700	0.37 ± 0.03	25.34 ± 0.17
H02	-5	1	26.0	204	700	0.36 ± 0.04	25.31 ± 0.17
H03	-7	1	15.7	174	600	0.35 ± 0.04	25.26 ± 0.18

Table 6. Merging of ellipticals lying on the KR.

Run	$\hat{E}$	$\hat{L}$	$20T_{\rm cr}$	$T_{\rm end}$	log $R_{\rm e}$ (kpc)	$\langle\mu_{\rm e}\rangle$
Progenitor (*KR*)					0.18 ± 0.00	19.00 ± 0.01
P01	-3	1	7	18	0.44 ± 0.03	19.54 ± 0.13
P02	-5	1	6	18	0.39 ± 0.02	19.30 ± 0.11
P03	-7	1	5	18	0.35 ± 0.02	19.08 ± 0.11
$P01_2$	-3	1	11	22	0.66 ± 0.04	19.92 ± 0.20
$P02_2$	-5	1	8	24	0.56 ± 0.04	19.41 ± 0.19
$P03_2$	-7	1	6	20	0.49 ± 0.04	19.01 ± 0.21

Table 7. Merging of ellipticals lying above the KR in the $\langle\mu_{\rm e}\rangle$–$R_{\rm e}$ plane.

Run	$\hat{E}$	$\hat{L}$	$20T_{\rm cr}$	$T_{\rm end}$	log $R_{\rm e}$ (kpc)	$\langle\mu_{\rm e}\rangle$
Progenitor (*AKR*)					0.19 ± 0.00	16.03 ± 0.00
A04	-3	1	1.74	8	0.44 ± 0.02	16.55 ± 0.12
A05	-5	1	1.46	6	0.39 ± 0.02	16.28 ± 0.11
A06	-7	1	1.42	6	0.34 ± 0.02	16.05 ± 0.10
A07	-3	2	1.74	8	0.44 ± 0.02	16.53 ± 0.11
A08	-5	2	1.46	6	0.38 ± 0.02	16.26 ± 0.11
A09	-7	2	1.26	6	0.34 ± 0.02	16.04 ± 0.11

[$T_{\rm cr} = GM^{5/2}/(2\ E)^{3/2}$]. The values for this time-scale are given in Tables 2–7, column (5).

Tables 2–7 summarize the initial conditions and characteristic parameters of the simulations. In Table 2, the mergers of one-component equal mass galaxies are labelled as follows.

(i) E01 – E13. *First-generation mergers*: simulations of the encounter of two single-component equal mass progenitors with different pairs of ($\hat{E}$, $\hat{L}$).

(ii) $E01_2$ – $E09_2$. *Second-generation mergers*: simulations of the encounter of two identical end-products of first generation mergers from the previous set of simulations. Progenitors are selected such that $E0i_2 = (E0i + E0i)$, with $i = \{1, 2, 5, 6, 8, 9\}$.

(iii) $E01_3$ – $E09_3$. *Third-generation mergers*: encounters between two identical second generation mergers with the progenitors selected such that $E0i_3 = E0i_2 + E0i_2$, with $i = \{1, 2, 5, 6, 9\}$.

The other simulations (Tables 3–7) with similar subscripts but a different starting letter, are as follows.

(i) D – mergers of different mass one-component mass galaxies.
(ii) F – mergers of UCD models.
(iii) H – mergers of two-component equal mass galaxies.
(iv) P – mergers of one-component models lying *on* the KR.
(v) A – mergers of one component models lying *above* the KR.

In Table 6, $P01_2$–$P03_2$ are the second-generation mergers which, as for the E mergers, had progenitors selected such that $P0i_2 = (P0i + P0i)$, with $i = \{1, 2, 3\}$. Similarly, in Table 4, $F01_j = (F01_{j-1} + F01_{j-1})$, where $j = \{2, 3, 4\}$.

Columns (2) and (3) in Tables 2–7 give the initial dimensionless orbital energy and corresponding angular momentum. Columns (4) and (6) give $T_{\rm per}$, the predicted time interval before the two-body

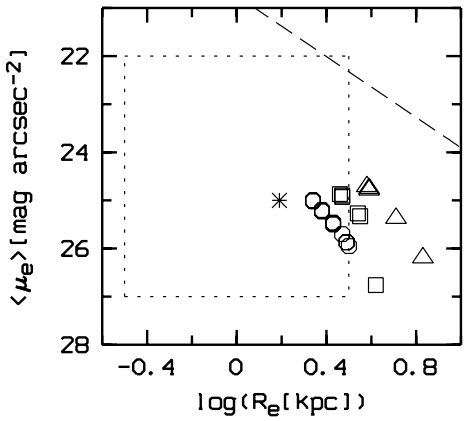

Figure 2. Merging of equal mass progenitors. Asterisk – the initial progenitor; circles – the first-generation progenitors; squares – the second-generation progenitors; triangles – the third-generation progenitors. The dashed line corresponds to the line in Fig. 1 that encompasses the region of bright ellipticals below and it is parallel to the KR. The rectangular area embraces the locus of the dwarf galaxies (see Fig. 1).

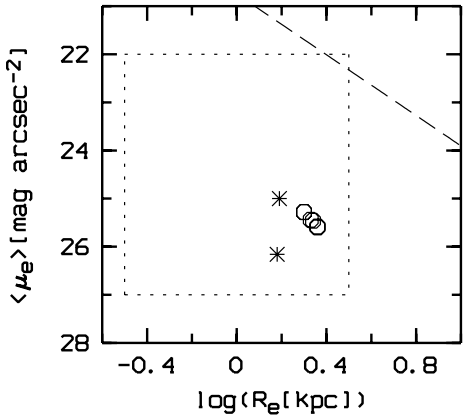

Figure 3. Same as in Fig. 2 but for merging of two different mass progenitors.

pericentre, and $T_{\rm end}$, the total time elapsed to the end of the simulation, respectively.

3 RESULTS

We followed the procedure described in Capelato et al. (1995) to quantify the observables involved in the KR: the effective radius $R_{\rm e}$, containing half of the total projected mass of the system, and the mean surface density within $R_{\rm e}$, $\Sigma_{\rm e} = M(<R_{\rm e})/\pi R_{\rm e}^2$, so that $\langle\mu_{\rm e}\rangle = -2.5\log\Sigma_{\rm e}$. These quantities were estimated as the median of 500 random projections. The errors quoted for each parameter are the rms based on the quartiles of the distribution defined by the 500 random projections. Columns (7) and (8) in Tables 2–7 list $R_{\rm e}$, the effective radius, and $\langle\mu_{\rm e}\rangle$, the mean surface brightness inside $R_{\rm e}$, for the merger remnant of each simulation. These quantities are shown in Figs 2–7.

In Table 2, the values of $\hat{E}$ and $\hat{L}$ defining the encounter span the region of rapid merging in the $\hat{E}$–$\hat{L}$ diagram (Binney & Tremaine 1987). Although arbitrary, this choice allows us to examine a particular scenario where mergers occur over a short time-scale. Some global trends can be seen from this set of simulations. First, $\langle\mu_{\rm e}\rangle$ always increases (lower surface brightness) with $R_{\rm e}$, and the rate of increase depends on the initial orbital energy. Secondly, the presence of angular momentum in the initial conditions does not significantly change the properties of the merger remnants, a trend already noted by Capelato et al. (1995). Therefore, we restrict ourselves to a smaller range of $\hat{L}$ for each $\hat{E}$ value in the further simulations described here. We use the same ($\hat{E}$, $\hat{L}$) for the simulations presented

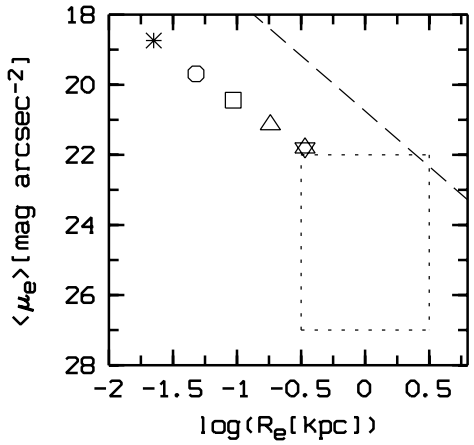

Figure 4. Same as in Fig. 2 but for merging of ultracompact dwarf galaxies.

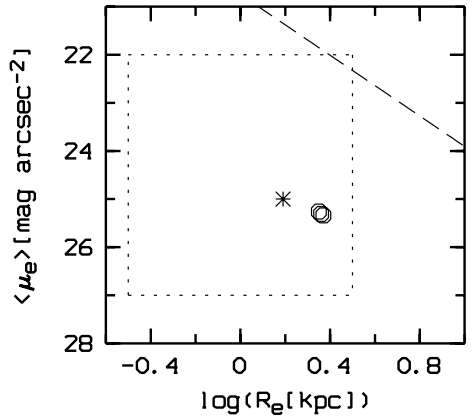

Figure 5. Same as in Fig. 2 but for merging of two equal mass progenitors with dark halo.

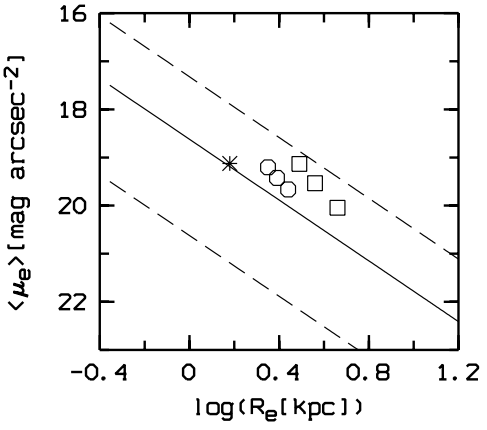

Figure 6. Merging of ellipticals lying on the KR. Asterisk – the initial progenitor; circles – the first-generation progenitors; squares – the second-generation progenitors. The dashed lines correspond to those in Fig. 1.

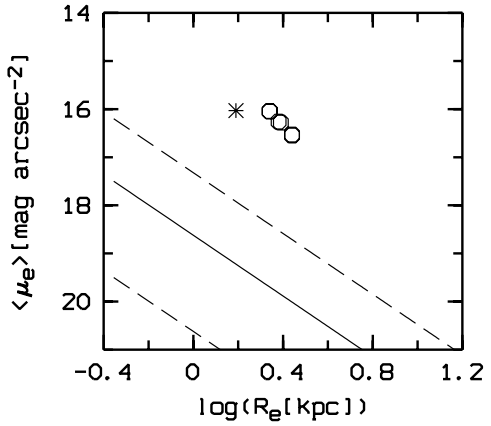

Figure 7. Merging of ellipticals lying above the KR in the $\langle\mu_e\rangle$–R_e plane. Asterisk – the initial progenitor; circles – the first-generation progenitors. The solid line represents the KR. The dashed lines correspond to those in Fig. 1.

in Tables 3–7 as for those in Table 2, except for the $\hat{E} = -1$ case included in Table 2, for which $T_{\rm per}$ is very large compared with the other simulations.

In the simulations presented in Tables 3–7 we restrict ourselves only to the first generation (except for the merging of objects lying on the KR – Table 6, and the merging of UCD models – Table 4), since the objects produced in the first generation tend always to move in the same direction in the $\langle\mu_e\rangle$–R_e plane as the first-generation systems listed in Table 2. Judging by the behaviour of the the second- and third-generation families displayed in Fig. 2, we can safely assume that further merging will also move the end-products to the bottom right in the $\langle\mu_e\rangle$–R_e plane.

4 DISCUSSION

In Capelato et al. (1995), the progenitors were systems of $M = 10^{11}$ $M_\odot$, while in this work we have used low-mass progenitors ranging from 0.6×10^8 to 9×10^8 $M_\odot$, since the main goal was to study whether or not the low-mass systems also move along the FP. However, the loci of the progenitors studied here are not along the KR (a projection of the FP). From our simulations, we see that present-day ellipticals cannot be formed by merging present-day dwarfs, unless a considerable amount of dissipation is involved. This result, together with other inconsistencies present in the properties of dwarfs and bright galaxies (see Tosi 2003), makes it nearly impossible that the major building blocks of present-day ellipticals had properties similar to those of dwarfs galaxies observed today.

The global trend observed in Figs 2–7 is that the end-products move down and right in the $\langle\mu_e\rangle$–R_e plane. On one hand, this shows that the only way to merge dwarfs and obtain bright ellipticals is by invoking a large amount of dissipation. On the other hand, the same trend suggests the possibility of making dwarfs by merging UCDs (clearly shown in Figs 4 and 8), as well as the possible formation of UCDs and dwarfs by merging globular clusters. Fellhauer & Kroupa (2002) have also shown that objects such as UCDs can be formed by merging globular clusters. Interestingly, in the dissipationless simulations by Dantas et al. (2003), the line going through the positions of the mergers of all of their three generations with $-4 < \hat{E} < +0.5$ has the same slope as the KR. However, their simulations do not reconstruct the KR entirely. In essence, all these

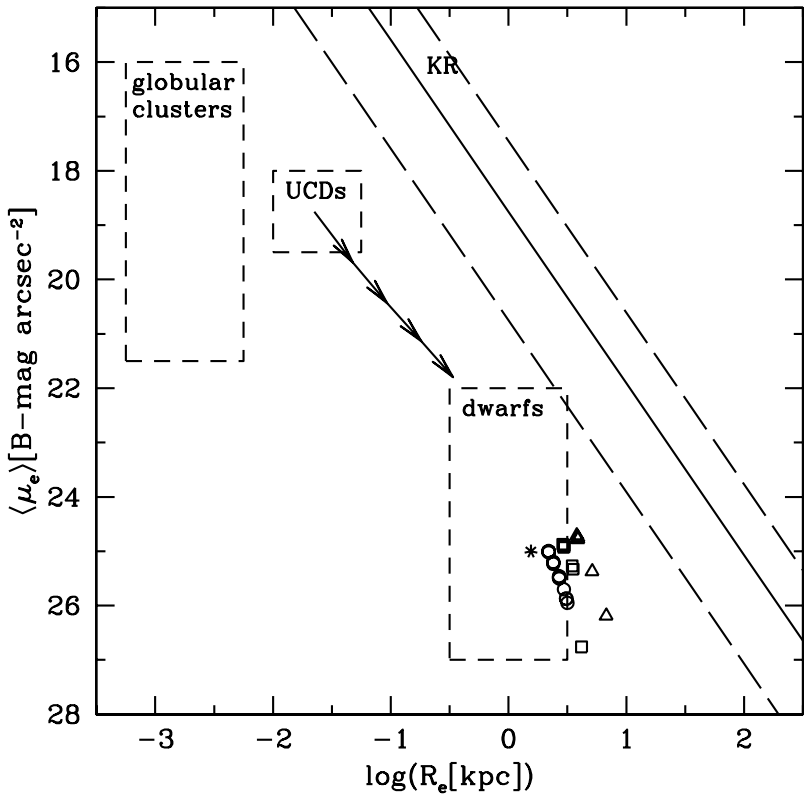

Figure 8. The evolution of dwarf galaxies in the $\langle\mu_e\rangle$–R_e plane. Merging of ultracompact dwarf galaxies is shown by large arrows. Different symbols represent the evolution of a dwarf galaxy due to the effects of dissipationless encounters for three subsequent merger generations. The solid line represents the Kormendy relation. Both long-dashed lines correspond to those in Fig. 1 which define the lower and the upper boundaries for bright ellipticals.

results show how dissipationless merging moves the systems in the $\langle\mu_e\rangle$–R_e plane, regardless of their mass.

The structural parameters of the end-products seem to strongly depend on the initial orbital parameters ($\hat{E}$, $\hat{L}$, and A). A recent study done by Khochfar & Burkert (2003) on the orbital parameters of major mergers of CDM haloes indicates that most of the encounters are nearly parabolic. However, as shown by simulations E11, E12 and E13, which correspond to parabolic and hyperbolic orbits, the trend is the same as observed for the other cases, namely, the end-products still move down and right in the $\langle\mu_e\rangle$–R_e plane. The global trend is independent of the $\hat{E}$ range, no matter what kind of orbits we consider.

The simulations where dark haloes were added to the low-mass spherical galaxies show that the merger remnants also shift down and right in the $\langle\mu_e\rangle$–R_e plane (Table 5 and Fig. 5), indicating that the presence of dark haloes does not make any appreciable difference as far as the global trend we find is concerned.

We also simulated the merging of a pair of objects lying on the KR. The end-products also lay on the KR within the scatter of the observed KR, and taking into account the simulation errors (Table 6 and Fig. 6), are in agreement with the results obtained by Capelato et al. (1995), and Dantas et al. (2003). The simulations where the progenitors were above the KR relation yielded the same overall result, moving down and to the right in the $\langle\mu_e\rangle$–R_e plane.

In Fig. 8 we show with different symbols the evolution of a progenitor due to the effects of dissipationless encounters (see Table 2 and Fig. 2) for three subsequent merger generations. The resultant vectors point to the locus of the bright ellipticals defining the KR. From the scheme presented in Fig. 8 we see that we cannot obtain a bright elliptical by merging low surface brightness ($\langle\mu_e\rangle = 25$–26) dwarfs. However, it is possible to reach the KR for bright ellipticals by merging higher surface brightness dwarf galaxies ($\langle\mu_e\rangle =$ 22–23) in a few (two or three) merger episodes, in agreement with Bower, Kodama & Terlevich (1998). We can imagine that at the initial merging stages, the main interaction process in the dwarfs is due to dissipational effects. In the $\langle\mu_e\rangle$–R_e diagram, this process is primarily represented by the upward movement of the dwarfs. Then, when these dwarfs reach the upper part of the dwarf locus, they will move according to the scheme in Fig. 8.

There are some caveats that should be noted. Dissipation could have a significant impact on the final position of an end product. Also, it is important to bear in mind that our simulations start from equilibrium systems representing a realization of a system that was previously formed. Moreover, the present merger rate differs from the one that applied in the past.

We plan on doing more extensive simulations using different models for the initial low-mass ellipticals (e.g. the exponential model or the more general Sersic's law) as well as those for the dark halo. To study how the initial spin of our models could affect the end products is also an important part of the future development.

ACKNOWLEDGMENTS

EAE was supported by Grants for Young Scientists PD 0.2-1.2-1 and MK – 2671.2003.02. EAE thanks V. P. Reshetnikov, N. Ya. Sotnikova and S. A. Rodionov for their assistance. RdC thanks Roy Gal and Gary Mamon for their careful reading of the manuscript, which helped to improve the content of this paper. We thank L. Hernquist for providing us with the code for realizations of the progenitors used in our simulations. We are also grateful to M. Drinkwater for the data on UCDs that he shared with us. HVC acknowledges financial support provided by CNPq and FAPESP. We thank the anonymous referee for very useful suggestions which helped to clarify some issues discussed in this paper.

REFERENCES

Barnes J., Hut P., 1986, Nat, 324, 446
Bekki K., Couch W. J., Drinkwater M. J., 2001, ApJ, 522, L105
Binney J., Tremaine S., 1987, Galactic Dynamics. Princeton Univ. Press, Princeton NJ
Burstein D., Bender R., Faber S. M., Nolthenius R., 1997, AJ, 114, 1365
Bower R. G., Kodama T., Terlevich A., 1998, MNRAS, 299, 1193
Capaccioli M., Caon N., D'Onofrio M., 1992, MNRAS, 259, 323
Capelato H. V., de Carvalho R. R., Carlberg R. G., 1995, ApJ, 451, 525
Cole S., Lacey C. G., Baugh C. M., Frenk C. S., 2000, MNRAS, 319, 168
Dantas C. C., Capelato H. V., Ribeiro A. L., de Carvalho R. R., 2003, MNRAS, 398, 428
Dantas C. C., Capelato H. V., de Carvalho R. R., Ribeiro A. L., 2002, A&A, 384, 772
de la Rosa I. G., de Carvalho R. R., Zepf S., 2001, AJ, 122, 93
Djorgovski S., Davis M., 1987, ApJ, 313, 59
Dressler A., Lynden-Bell D., Burstein D., Davis R. L., Faber S. M., Terlevich R., Wegner G., 1987, ApJ, 313, 42
Drinkwater M. J., Jones J. B., Gregg M. D., Phillipps S., 2000, PASA, 17, 227
Drinkwater M. J., Gregg M. D., Hilker M., Bekki K., Couch W. J., Ferguson H. C., Jones J. B., Phillipps S., 2003, Nat, 423, 519
Dubinski J., 1988, MS thesis Univ. Toronto
Eggen O. J., Lynden-Bell D., Sandage A. R., 1962, ApJ, 136, 748
Faber S. M., Jackson R. E., 1976, ApJ, 204, 668
Fellhauer M., Kroupa P., 2002, MNRAS, 330, 642
Graham A. W., Guzman R., 2003, AJ, 125, 2936
Grebel E. K., 2001, in de Boer K. S., Dettmar R. J., Klein U., eds, Dwarf Galaxies and their Environment, Bad Honnef Workshop. Shaker Verlag, Aachen
Grebel E. K., Gallagher J. S., Harbeck D., 2003, AJ, 125, 1926
Hernquist L., 1990, ApJ, 356, 359
Hernquist L., 1993, ApJS, 86, 389
Kauffmann G., 1996, MNRAS, 281, 487
Khochfar S., Burkert A., 2003, preprint (astro-ph/0309611)
Klypin A., Kratsov A. V., Valenzuela O., Prada F., 1999, ApJ, 522, 82
Kormendy J., 1977, ApJ, 218, 333
Larson R. B., 1975, MNRAS, 173, 671
Merritt D., 1996, AJ, 111, 2462
Moore B., Ghigna S., Governato F., Lake G., Quinn T., Stadel J., Tozzi P., 1999, ApJ, 524, L19
Nipoti C., Londrillo P., Ciotti L., 2003, MNRAS, 342, 501
Prantzos N., Silk J., 1998, ApJ, 507, 229
Tolstoy E., Venn K. A., Shetrone M., Primas F., Hill V., Kauffer A., Szeifert T., 2003, AJ, 125, 707
Tosi M., 2003, Ap&SS, 284, 651
White S. D. M., Rees M. J., 1978, MNRAS, 183, 341

This paper has been typeset from a TEX/LATEX file prepared by the author.